Hindawi Publishing Corporation
Journal of Nanomaterials
Volume 2014, Article ID 293624, 10 pages
http://dx.doi.org/10.1155/2014/293624

Research Article

A Dual-Functional [SBA-15/Fe_3O_4/P(*N*-iPAAm)] Hybrid System as a Potential Nanoplatform for Biomedical Application

Andreza de Sousa,[1,2] Karynne Cristina de Souza,[1] Paula Maria da Silva Leite,[1,2] Ricardo Geraldo de Sousa,[2] and Edésia Martins Barros de Sousa[1]

[1] *Serviço de Nanotecnologia, Centro de Desenvolvimento da Tecnologia Nuclear CDTN/CNEN, Avenida Presidente Antônio Carlos, 6.627, Campus da UFMG, Pampulha, 31270-90 Belo Horizonte, MG, Brazil*
[2] *Departamento de Engenharia Química, E.E.UFMG, Avenida Presidente Antônio Carlos, 6.627, Campus da UFMG, Pampulha, 31270-90 Belo Horizonte, MG, Brazil*

Correspondence should be addressed to Edésia Martins Barros de Sousa; sousaem@cdtn.br

Received 15 November 2013; Revised 7 February 2014; Accepted 23 February 2014; Published 3 April 2014

Academic Editor: Anchal Srivastava

The synthesis strategy of a multifunctional system of [SBA-15/Fe_3O_4/P(*N*-iPAAm)] hybrids of interest for bioapplications was explored. Magnetite nanoparticles coated by mesoporous silica were prepared by an alternative chemical route using neutral surfactant and without the application of any functionalization method. Monomer adsorption followed by *in situ* polymerization initiated by a radical was the adopted procedure to incorporate the hydrogel into the pore channels of silica nanocomposite. Characterization of the materials was carried out by using X-ray diffraction (XRD), Fourier-transform infrared spectroscopy (FTIR), N_2 adsorption, transmission electron microscopy (TEM), and Temperature programmed reduction studies (TPR). Their application as drug delivery system using atenolol as a model drug to assess the influence of the application of low frequency alternating magnetic fields on drug release was evaluated. The structural characteristics of the magnetic hybrid nanocomposite, including the effect of the swelling behavior on heating by the application of an alternating magnetic field, are presented and discussed.

1. Introduction

Ordered mesoporous materials have a number of promising applications in many fields of technology as advanced electronics, catalysis, and nanostructured materials, among others [1–3]. The intrinsic uniform porous structure of this class of compounds with their large specific surface area and pore volume, associated with surface silanol groups, give these materials a significant potential for applications as matrices of many chemical species, such as organic molecules, metals, and polymeric materials. The performance of these materials in many fields of applications depends directly on the silica network porosity. Because of their large pores, high hydrothermal stability, and easy preparation, SBA-15 materials have been considered very promising for hosting and further delivery under appropriate conditions of a variety of molecules of pharmaceutical interest [4].

The delivery of these molecules was once considered impossible, because of the difficulty associated with the diffusion of large molecules through the materials of conventional drug delivery systems. These organic substances are normally very large in size and mesoporous silica is a potential candidate to encapsulate such molecules by utilizing ordered mesopores [5, 6]. Nevertheless, there is one major problem for the mesoporous systems as far as drug release is concerned, that is, the limited control of the drug release whose major mechanism is diffusion [7]. The need to create new materials with optimized, predetermined characteristics has spurred an increasing interest in hybrid materials, especially in organic and inorganic nanocomposites.

For a better release control, some systems can be externally activated to release more drugs when necessary using external forces such as temperature or magnetism [8].

In the case of temperature aging as an external force for diffusion, temperature-responsive hydrogels are a well-studied class of drug delivery systems, as they can respond pronouncedly to temperature changes. Among these stimuli-responsive polymers, temperature-responsive hydrogels such as poly(*N*-isopropylacrylamide) [P(*N*-iPAAm)] [9, 10] exhibits, in water, a phase transition at a lower critical solution temperature (LCST) of approximately 33°C [11]. Below the LCST, the hydrogel incorporates water and swells, whereas the release of water in response to an increase in temperature causes shrinkage. Thus, the development of hybrid functional nanosystems based on silica-[P(*N*-iPAAm)] has drawn much attention to the control of molecular transport, including drug release, because self-regulated delivery allows for drug release when it is needed [5]. Such a thermosensitive polymer with reversible phase transition characteristics is attractive as a polymeric material for the temperature responsive drug release systems [12].

In the case of magnetism, the magnetite nanoparticles can be used to target localized heating *in vivo* when an alternating current (AC) magnetic field is applied, like in the hyperthermia treatment for anticancer therapy due their unique magnetic properties [13]. This treatment consists in dispersing the magnetic nanoparticles in the diseased tissue and applying an alternating magnetic field to cause local heating. Temperature around 43–45°C lysis the tumor cells with no damage to normal cells. However, nonsurface-modified magnetic nanoparticles with a large surface-area-to-volume ratio tend to agglomerate and form large clusters, with the consequent loss of interesting characteristics. Therefore, a suitable coating is essential to prevent such limitations, what can be obtained by using mesoporous silica like SBA-15. For SBA-15/Fe_3O_4, it is possible to obtain magnetite nanoparticles embedded into mesoporous silica, preventing the agglomeration [14]; these coatings provide not only the stability to the nanoparticles in solution but also helps in binding the various biological ligands at the nanoparticle surface for various biomedical applications [15].

Considering a multifunctional system composed by silica/magnetite/gel, a magnetic field with an alternating current (AC) can be used to target localized heating *in vivo* through the magnetohyperthermia treatment for anticancer therapy, which in turn causes a phase change in the host polymer to allow diffusion and release of drugs. In this case, the thermosensitive grafts collapse, opening pathways for an imbedded drug into the system to escape [16]. Thus, an important improvement in cancer therapy would allow two modes of treatment with synergistic effects of magnetic hyperthermia and drug release using a single hybrid system consisting of silica/magnetite/poly(*N*-isopropylacrylamide).

Even though there have been significant advances, studies involving the potential use of responsive hybrids in the area of controlled release of drugs in synergism of magnetohyperthermia are still incipient, many properties of these materials are in the process of analysis, and synthesis procedures are being modified in order to gain greater control over these morphological and structural materials.

In view of the aforementioned, the objective of this study was to investigate the synthesis strategy of a dual-functional system of [SBA-15/Fe_3O_4/P(*N*-iPAAm)] hybrids of interest for bioapplications. Magnetite nanoparticles coated by mesoporous silica were prepared by an alternative chemical route using neutral surfactant and without the application of any functionalization method. Monomer adsorption followed by *in situ* polymerization initiated by a radical was the adopted procedure to incorporate the hydrogel into the pore channels of silica nanocomposite. Subsequently, its physicochemical characteristics were investigated by using different techniques and the drug release profile of the system was studied in the presence of magnetic field-induced heating. In addition, the effects of the gel swelling behavior on heating by the application of an alternating magnetic field were also presented and discussed in terms of drug release and heat generation capacity.

2. Experimental

2.1. Material Synthesis. SBA-15 was synthesized in accordance with the published procedure [17] using Pluronic P123-$PEO_{20}PPO_{70}PEO_{20}$ (poly(ethylene glycol)-block-poly (propylene glycol)-blockpoly (ethylene glycol), M_{av} = 5800, Sigma-Aldrich) as a template in acidic conditions. In a typical experiment, 4 g of triblock copolymer was dissolved in water and HCl (37 wt. % solution) under stirring at 40°C. After 1 h, 8.2 g of tetraethyl orthosilicate (TEOS, Sigma-Aldrich) was added to the solution. After aging under continuous stirring at 100°C, the solids were collected by filtration and dried in air at 40°C. The surfactant was removed by calcination, which was carried out by increasing the temperature to 550°C under nitrogen flow for 2 h and then in O_2 atmosphere for another 1 h. SBA-15/Fe_3O_4 was prepared by adding 4 g of iron oxide precursor ($Fe_2(SO_4)_3 \cdot 6H_2O$) before the addition of TEOS in the synthesis of silica SBA-15. The step of surfactant removing was carried out by heating the material in a nitrogen atmosphere at a rate of 5°C min^{-1} to 550°C. At this temperature the material was kept under nitrogen flow for 8 hours. The nitrogen flow remained constant throughout the heating process and followed up to complete cooling of the sample. The hybrid was prepared using the following procedure: 0.5 g of SBA-15/Fe_3O_4 nanocomposite was added to 3.5 mL solution of 0.245 g of monomer (*N*-isopropylacrylamide—*N*-iPAAm) and 0.005 g of crosslinking agent (N,N,N′,N′—methylene-bisacrylamide—MBA). The mixture was transferred to an INNOVA 4200 (150 rpm) shaker and the mixture was continuously purged with nitrogen. The solution was then allowed to polymerize for 24 h in a water bath at 9°C. The obtained multifunctional hybrid material was dried at 60°C for 24 h and subsequently washed to remove the excess monomers, crosslinking agent, initiator, and accelerator. In the washing stage, the material was disaggregated, suspended in water, and continuously stirred. The hybrid was then collected by centrifugation at 3600 rpm for 3 min and dried at 60°C for 24 h. It was designated [SBA-15/Fe_3O_4/P(*N*-iPAAm)] and the gel composition studied was 5 × 1 [7]. The monomer: SBA-15 mass ratio used was 1 : 2 (wt/wt).

2.2. Characterization. The samples were characterized by X-ray diffraction (XRD), Fourier-transform infrared spectroscopy (FTIR), N_2 adsorption, transmission electron microscopy (TEM), and Temperature programmed reduction studies (TPR). Low-angle XRD measurements were obtained using synchrotron radiation with $\lambda = 1.488$ nm. Synchrotron radiation measurements were carried out at the D11A-SAXS beamline of the LNLS (Campinas, Brazil) using a Huber-423 3-circle diffractometer. The high-angle XRD patterns were obtained using a Rigaku Geigerflex-3034 diffractometer with a Cu-Kα tube. Specific surface area and pore size distribution were determined by N_2 adsorption using the BET and BJH methods, respectively [18], in Autosorb-Quantachrome Nova 1200. The samples were outgassed for 2 h at 120°C before analysis. FTIR measurements were conducted in a Perkin-Elmer 1760-X spectrophotometer in the range 4000–400 cm^{-1} at room temperature using KBr pellets. TEM characterization was performed through a Tecnai-G2-20-FEI 2006 electron microscope with an acceleration potential of 200 kV, of the Microscopy Center of UFMG, Belo Horizonte, Brazil. TPR experiments were performed in a CHEMBET 3000 equipment with 20 mg sample under 25 mL min^{-1} H_2 (8%)/N_2 with heating rate of 5°C min^{-1}.

2.3. Calculations. BET specific surface area, S_{BET}, was calculated from adsorption data in the relative pressure interval $p/p_0 = 0.045–0.25$. A cross-sectional area of 0.162 nm^2 was used for the nitrogen molecule in the BET calculations. The total pore volume, V_p, was calculated from the amount of N_2 adsorbed at the highest p/p_0 ($p/p_0 = 0.99$) [19]. The micropore volume, V_μ, of SBA-15 silica was estimated from nitrogen adsorption data using the α_s plot method [20] in the standard reduced adsorption, α_s, interval from 0.75 to 1 (relative pressure range from 0.15 to 0.40). The external surface area, S_{ext}, was evaluated using an α_s interval from 1.6 to 3.0. The primary mesopore volume, V_{meso}, was estimated as the difference between the total pore volume and the micropore volume. The α_s-plot was analysed by standard reduced adsorption for nonporous hydroxylated silica [21]. The mesopore size distributions were calculated from the adsorption branches of the nitrogen isotherms employing the BJH algorithm.

2.4. Model Drug Adsorption and Delivery Assays. All samples were loaded with atenolol as a model drug as follows: 0.5 g of the powder sample was added to 150 mL of an atenolol solution (10 mg·mL^{-1}) and shaken for 48 h at 25°C (200 rpm). A 3 : 1 weight ratio of atenolol/solid sample was used. Powder atenolol loaded samples were recovered by filtration, washed with distilled water, and left to dry for 24 h at 60°C. The same procedure was used to load the hybrid with atenolol. Small atenolol loaded sample disks with 7 mm diameter and 2 mm thick were obtained under uniaxial pressure. TGA was performed to evaluate the percentage of atenolol adsorbed by each sample.

The *in vitro* study of release of atenolol from the materials was performed as follows. The release profile was obtained by soaking nanocomposites [SBA-15/Fe_3O_4] and hybrid [SBA-15/Fe_3O_4/P(*N*-iPAAm)] samples in 30 mL of simulated body fluid (SBF) [22]. The temperature was maintained constant (37°C) and the solutions were continually stirred. UV spectrometry (UV-Vis Shimadzu, model 2401) was used to monitor the amount of drug delivered as a function of time. The concentration of atenolol in SBF was found from the intensity of the absorption band at 274 nm.

2.5. Hyperthermia. The capacity of heat generation of the obtained nanocomposites and hybrid system was measured in a custom-designed magnetic-induction hyperthermia chamber. Heating was measured of [SBA-15/Fe_3O_4] and hybrid [SBA-15/Fe_3O_4/P(*N*-iPAAm)] samples dispersed in water with sonication. The sample concentration was 20 mg·mL^{-1} and the solution was sonicated for 30 min before measurement. A three-loop coil with resonant frequency of 222 kHz was used in the experiments. In order to study the correlation between the applied magnetic field and the AC magnetically induced heating temperature, the heat produced was measured at a fixed frequency in magnetic 126 Oe until the temperature was nearly steady. A digital thermometer was placed above the sample inside the coil and the temperature measurements were taken at the center of the sample. The results were the average of triplicate measurements. Tests have also been performed in pure deionized water without any magnetic material and the temperature increase from this blank sample has been subtracted of the results obtained for the solution.

2.6. Statistical Analysis. The results were calculated and presented as the mean for each group ± the standard error of the mean (mean ± SD). Statistical evaluation of the data was performed using analysis of variance (ANOVA), followed by Bonferroni's test (Post hoc), where $P \leq 0.05$ was considered to be statistically significant.

3. Results and Discussion

3.1. Material Characterization. Figure 1 shows the X-ray diffractograms of the pure magnetite prepared via oxidation-precipitation route, and SBA-15/Fe_3O_4 sample treated at 550°C. The broad diffraction peak at high angles (Figure 1(a)) at 2θ between 20° and 30° is attributed to the peak of the siliceous material. In addition, several XRD peaks indicate the formation of well-crystallized Fe_3O_4. The sharp main diffraction peak and other weak diffraction peaks at 2θ = 30.0°, 35.4°, 56.9°, and 62.4°, respectively, can be assigned to (220), (311), (511), and (440) reflections, which can be indexed to the spinel structure of pure stoichiometric magnetite (Fe_3O_4) (JCPDS file 19-0629).

SBA-15/Fe_3O_4 sample has been analyzed by temperature programmed reduction employing H_2 as reducing gas and the results are presented in Figure 2. TPR profile shows mainly three sets of reduction process. The consumption

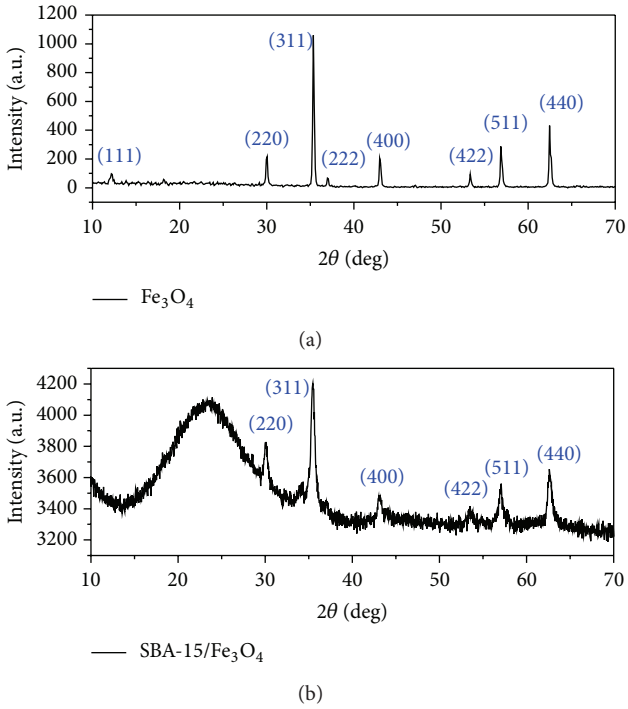

FIGURE 1: X-ray diffraction patterns of the pure magnetite and silica-magnetite nanocomposite.

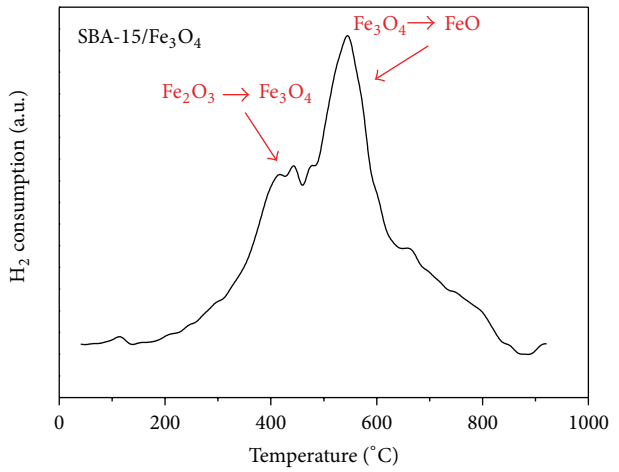

FIGURE 2: TPR profiles of the SBA-15/Fe_3O_4 sample.

profile of H_2 for this sample shows characteristic peaks of reduction transformation of the following phases [23]:

$$\begin{aligned} Fe_2O_3 &\longrightarrow Fe_3O_4 \,(\text{maghemite} \longrightarrow \text{magnetite}) \\ Fe_3O_4 &\longrightarrow FeO \,(\text{magnetite} \longrightarrow \text{wustite}) \end{aligned} \quad (1)$$

However, the largest nitrogen consumption was observed in the temperature range of 485–650°C, regarding the conversion of magnetite to wustita, confirming the hypothesis that the phase present in higher concentration is magnetite. It is worth mentioning that this sample does not contain ferrisilicate since it has no peaks at temperatures higher than 700°C that are characteristic of phase transformation of ferrisilicate.

Figures 3(a) and 3(b) show the profile at low angle for SBA-15/Fe_3O_4 and the [SBA-15/Fe_3O_4/P(*N*-IPAAM)], respectively. The three diffraction peaks of the former, at 2θ = 0.85°, 1.51°, and 1.75°, can be indexed as (100), (110), and (200) reflections, respectively, which are typical of hexagonally structured SBA-15 silica with highly ordered mesoporous channels, as reported by Zhao et al. [24]. However, a slight shift of these diffraction peaks to higher 2θ values is identified for [SBA-15/Fe_3O_4/P(*N*-IPAAm)], Figure 3(b), possibly due to the contraction of the support framework with the formation of the polymer phase in the silica channels. The XRD peaks of SBA-15/Fe_3O_4 can be indexed to a hexagonal lattice structure with $d(100)$ spacing of 9.5 nm and unit cell parameter ($a = 2d/\sqrt{3}$) of 10.94 nm, as reported by Souza et al. [25]. On the other hand, the d spacing of [SBA-15/Fe_3O_4/P(*N*-IPAAM)] shifted slightly to 9.2 nm, corresponding to a unit cell parameter of 10.62 nm. Despite these small differences in the reflections of the XRD peaks, it is clear that the mesostructure was still ordered after the polymer phase was loaded.

Figure 4 shows the TEM images of the [SBA-15/Fe_3O_4] and [SBA-15/Fe_3O_4/P(*N*-iPAAm)] hybrid samples. In accordance with the low angle XRD results, the mesoscopic order of the host can be clearly identified in the TEM image of both samples, which shows a well-defined hexagonal arrangement of uniform pores when the incident electron beam was parallel to the main axis of the mesopores (Figure 4(a)), and unidirectional channels, when the electron beam was perpendicular to the channel axis (Figure 4(b)). The Fe_3O_4 nanoparticles appear as dark dot-like objects between the channel walls (Figure 4(c)). These nanoparticles are evenly distributed in the channels with a uniform size, which is close to the pore diameter of SBA-15. Thus, the TEM investigation gives consistent evidence that the ordered structure is preserved in the approach proposed in this work to obtain a nanocomposite and hybrid systems.

Figure 5 shows the FTIR spectra of the SBA-15/Fe_3O_4 and the hybrid [SBA-15/Fe_3O_4/P(*N*-IPAAm)] samples before and after washing procedure to remove residual monomers. For SBA-15/Fe_3O_4 sample, the infrared spectrum shows absorption bands concerning to fundamental vibrations network of silica. The amount of water in the samples can be monitored by observing the adsorption lines at 3500 and 1640 cm^{-1}, whereas SiOH can be seen as a shoulder at 960 cm^{-1} for all spectra. The band at about 810 cm^{-1} is related to the symmetric stretching of the Si–O–Si and the band about 460 cm^{-1} is related to the vibration mode deformation Si–O–Si. A broad and very intense band in the range 1000–1200 cm^{-1} corresponding to νSi–O–Si modes of the siliceous matrix of SBA-15 is also present. The spectrum of SBA-15/Fe_3O_4 is dominated by νO–H modes, presenting a broad and intense band at 3440 cm^{-1} assigned to hydroxyl groups.

It can be seen in the spectrum of hybrid [SBA-15/Fe_3O_4/P(*N*-IPAAM)] systems before the washing procedure, bands corresponding to the ν_{C-H} modes of P(*N*-iPAAm) at 2972–2875 cm^{-1}, the bands attributed to isopropyl

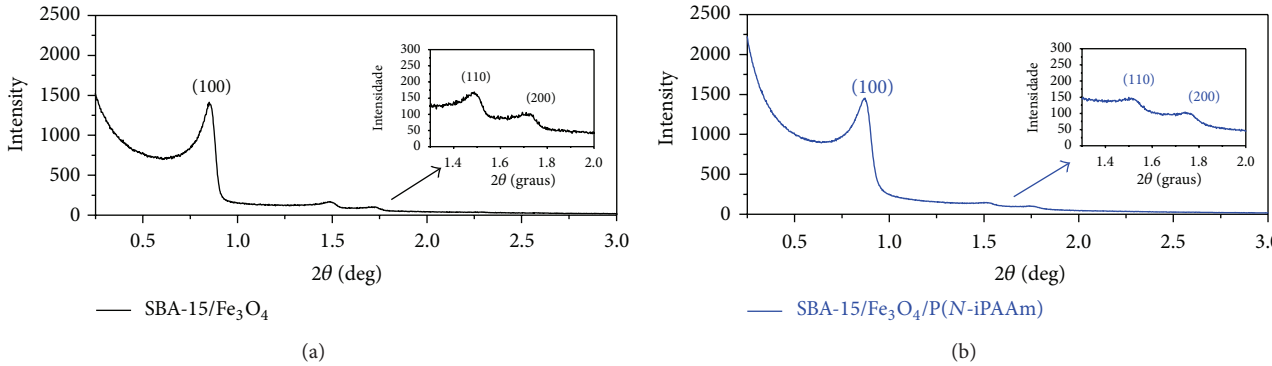

Figure 3: X-ray diffraction patterns of small-angle region of (a) SBA-15/Fe_3O_4 and (b) [SBA-15/Fe_3O_4/P(*N*-iPAAm)].

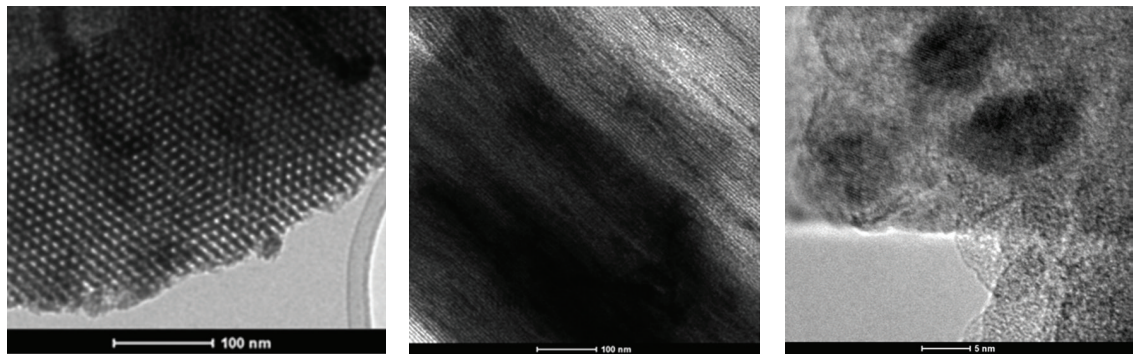

Figure 4: Transmission electron micrographs of [SBA-15/Fe_3O_4/P(*N*-iPAAm)]: (a) viewed along the pore axis, (b) viewed perpendicular to the pore axis, and (c) high resolution images showing the magnetite nanoparticles (dark region) covered by the mesoporous silica of SBA-15/Fe_3O_4.

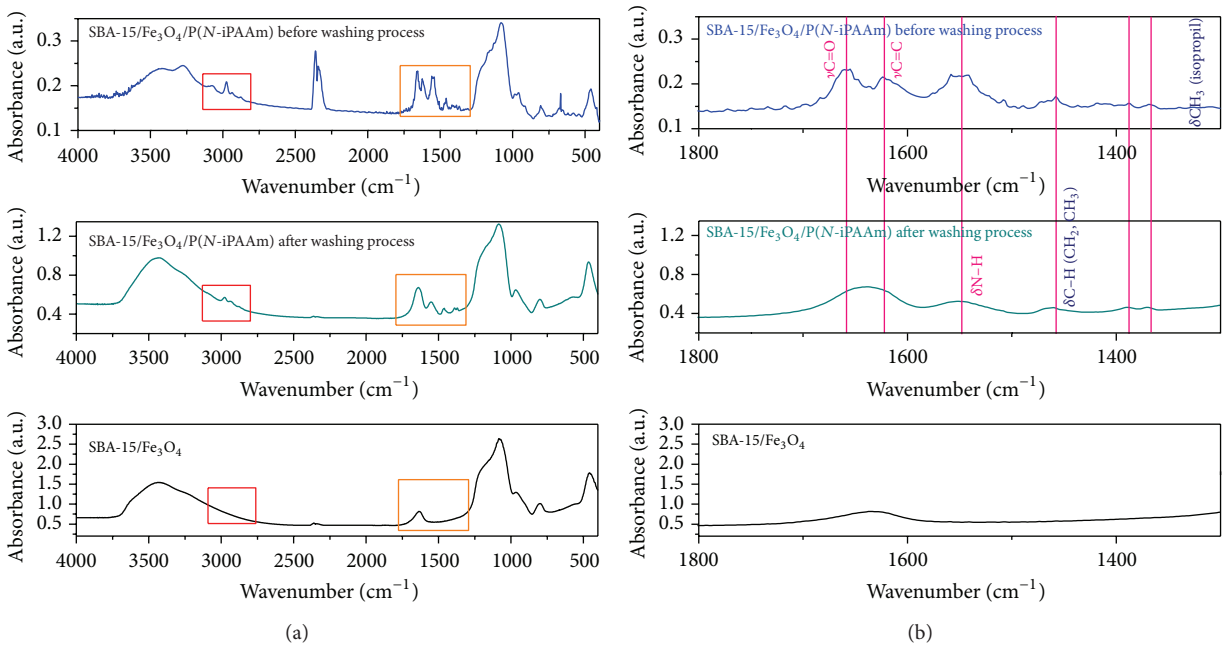

Figure 5: (a) FTIR spectra of SBA-15/Fe_3O_4 and [SBA-15/Fe_3O_4/P(*N*-iPAAm)] before and after the washing procedure to remove the residual monomers. (b) FTIR spectra of SBA-15/Fe_3O_4 and [SBA-15/Fe_3O_4/P(*N*-iPAAm)] before and after the washing procedure to remove the residual monomers in the expanded scale of 2000–1400 cm^{-1}.

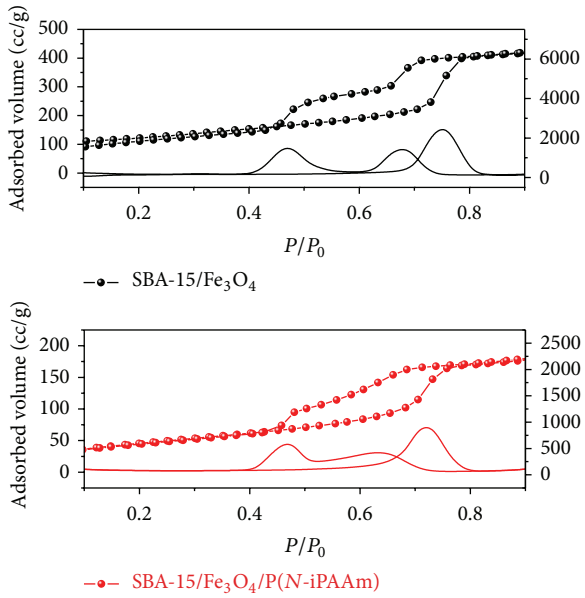

FIGURE 6: N_2 adsorption-desorption isotherms and respective derived curves of SBA-15/Fe_3O_4 and [SBA-15/Fe_3O_4/P(*N*-iPAAm)] hybrid system.

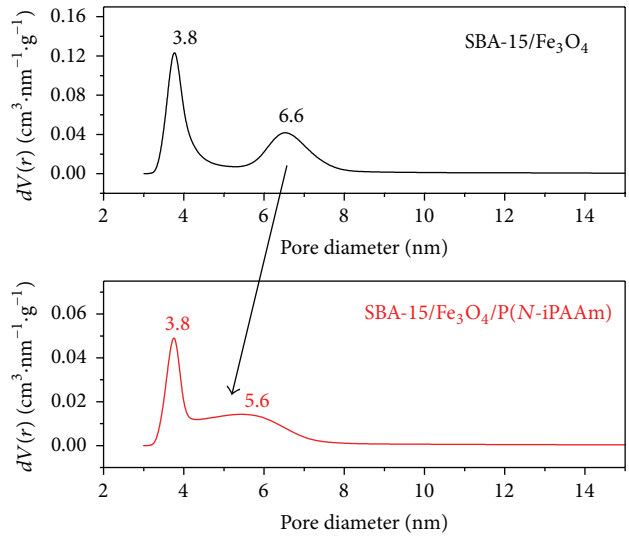

FIGURE 7: Pore size distribution of SBA-15/Fe_3O_4 and [SBA-15/Fe_3O_4/P(*N*-iPAAm)] hybrid system.

group are located at 1386 and 1368 cm^{-1}. The band corresponding to the bending vibration of CH_3 is located at 1456 cm^{-1}, while the bands arising from C=O stretching and N–H bending vibrations are observed at 1645 and 1550 cm^{-1}, respectively.

The monomer characteristic bands (νC=C 1620 cm^{-1}, δCH_2 = 1409 cm^{-1}, δH_2C=C– 1305, and 1325 cm^{-1}, δvinyl group at 990 and 916 cm^{-1}) are not present in the hybrid sample spectra, as can be seen in the scale-expanded FTIR spectrum in the 1800–900 cm^{-1} region (Figure 5(b)). These results prove the presence of P(*N*-iPAAm) in SBA-15/Fe_3O_4 pores with no other significant synthesis components (monomer, initiator, or accelerator) and demonstrate the successful conversion of the monomers into polymer and the removal of the residual monomers. In addition, the stretching bands of carbonyl groups and N–H bending vibrations from secondary amide around 1648 and 1550 cm^{-1}, respectively, in the spectrum of the sample after washing, are broader compared to the spectrum before washing, likely due the intramolecular interactions such as hydrogen bond (C=O $\cdots$ HN) which can occur between the polymer chains after the polymerization reaction.

The nitrogen adsorption isotherms for SBA-15/Fe_3O_4 and the [SBA-15/Fe_3O_4/P(*N*-iPAAm)] hybrid are shown in Figure 6. In both cases, the isotherms were type IV, according to the IUPAC classification, which is associated with the presence of mesopores [19]. These H1 type hysteresis isotherms are related to materials with pores of uniform cross section (e.g., cylindrical or hexagonal). However, these materials exhibit the phenomenon of stepwise desorption, often referred to as blocking phenomenon of pores and is typically associated with the bottle-shaped pores (ink bottle pores) (Figure 6).

Antochshuk and coauthors [26] attributed this stepwise desorption phenomenon due to the presence of constrictions in the porous structures. According to the authors, in the case of a pore connected to neighboring pores or its surroundings through entrances (constrictions) with diameter smaller than the pore diameter, capillary evaporation from the pore interior is delayed until the capillary evaporation from the constrictions takes place. This phenomenon can be more easily seen in the curves derived from the adsorption and desorption branches (Figure 6). After polymerization, the shape of the hysteresis loop in the N_2-sorption isotherm displays a broadening suggestive of a reduction in pore size uniformity.

All samples present a bimodal pore size distribution due to the presence of mesopores of different diameters, for example, primary mesopores, secondary, or pores with constrictions. In Figure 7, it is possible to observe two maximum points for SBA-15/Fe_3O_4: one about 6.6 nm, corresponding to the primary mesoporosity, and the second corresponding to a diameter of 3.8 nm equivalent to the secondary mesoporosity. In the hybrid multifunctional, the first maximum point is shifted to lower values of diameter: 5.6 nm and no change were observed in the secondary mesopores, which kept on 3.8 nm.

It can be seen that the pore size distribution is affected by the incorporation of polymeric gel in the SBA-15/Fe_3O_4 sample. After incorporation of the gel, it fills the pores with higher diameters (peaks at 6.6 nm), reducing its statistical contribution and causing a shift of the maximum point for lower values of pore diameter. Notably, the incorporation of the gel does not cause complete filling of the pores of the final material. Even after incorporation of the gel into SBA-15/Fe_3O_4 samples, significant values of surface areas can be observed, which may be convenient to use this material as drug release devices (Table 1).

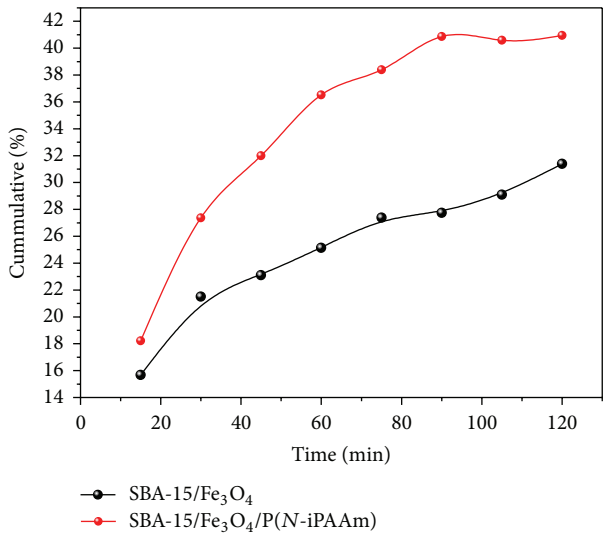

FIGURE 8: Release kinetic profiles of atenolol from SBA-15/Fe_3O_4 and [SBA-15/Fe_3O_4/P(*N*-iPAAm)] samples.

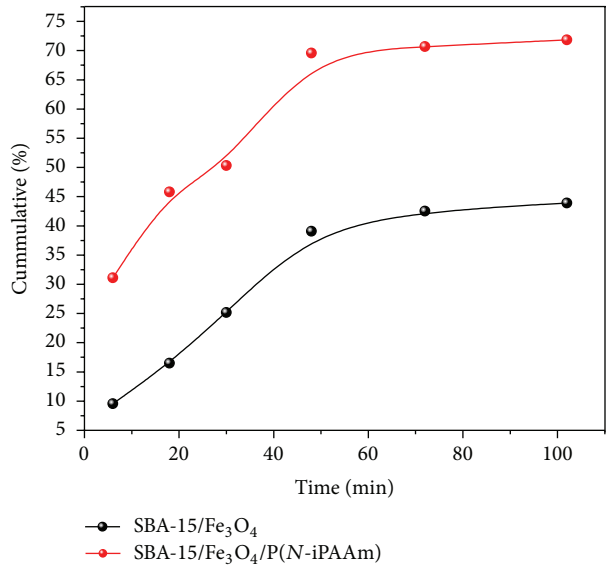

FIGURE 9: Release kinetic profiles of atenolol from SBA-15/Fe_3O_4 and [SBA-15/Fe_3O_4/P(*N*-iPAAm)] systems in an alternating field.

TABLE 1: N_2 adsorption results.

Sample	S_{BET} ($m^2 \cdot g^{-1}$)	V_p (cm^3/g)	$D_{p\,(BJH)}$ (nm)
SBA-15/Fe_3O_4	413	0.76	3.8/6.5
[(SBA-15/Fe_3O_4/P(*N*-iPAAm)]	171	0.35	3.8/5.6

Table 1 presents the results of N_2 adsorption, which show the differences in the specific surface area (S_{BET}), pore volume (V_p), and pore diameter (D_p) of the samples. A significant difference was observed for the S_{BET}, V_p, and D_p for SBA-15/Fe_3O_4 and [SBA-15/Fe_3O_4/P(*N*-IPAAM)] samples, which may indicate the presence of the polymer in the pore structure. Regarding the nitrogen adsorbed volume, it was found that the formation of P(*N*-IPAAM) into the mesoporous support provoked on a slight decrease in the pore volume and in the pore diameter.

3.2. Atenolol Incorporation and Release Profile Study. *In vitro* atenolol release properties from mesoporous SBA-15/Fe_3O_4 and [SBA-15/Fe_3O_4/P(*N*-iPAAm)] were investigated as a function of time and are shown in Figure 8. The resulting drug loading into samples was approximately the same, 41 wt% for SBA-15/Fe_3O_4 and 44 wt% for [SBA-15/Fe_3O_4/P(*N*-iPAAm)], as no statistically significant differences could be observed ($P > 0.05$) in the loading percentage. The release profiles of both samples exhibited no initial burst release effect during the first minutes. However, as can be observed from Figure 8, SBA-15/Fe_3O_4 sample did in fact release a smaller percentage of atenolol than did the hybrid sample. The maximum release level achieved in 2 hours for the SBA-15/Fe_3O_4 sample was 32% and for hybrid system was 43%.

As a result, the presence of the gel increased the amount of drug released, which shows the potential application of this material as a controlled release of drugs. It is relevant to mention here that the drug release rate can be enhanced using magnetic field, which would subsequently reduce the period for the drug release. Considering this fact, and in order to evaluate the multifunctionality of the SBA-15/Fe_3O_4 and [SBA-15/Fe_3O_4/P(*N*-iPAAm)] systems as release device via magnetic hyperthermia treatment, a preliminary test was carried out where the samples were subjected to an external magnetic field over the time. The study was based on the model proposed by Dash and Cudworth [27], in which the application of an alternating magnetic field provokes the vibration of the magnetic particles and the quick release of large quantities of drugs. The measures presented here are designed to assess the influence of the application of low frequency alternating magnetic fields (168 Oe) on drug release [28].

Figure 9 shows the result of this experiment for SBA-15/Fe_3O_4. The presence of magnetic field provokes a heating of the nanocomposite material due to the presence of magnetic particles; thus, the diffusion of atenolol molecules was enhanced by increasing the vibration of the nanoparticles and, consequently, increasing the amount of drug released.

The same behavior can be observed for hybrids systems. Similar to the experiment of release without the influence of the magnetic field, the presence of the gel into the nanocomposite structure increased the amount of drug released, and these results can be explained by the possible interaction of the drugs with the magnetite nanoparticles, maybe due to the incorporation of atenolol into the mesopores, and its interaction with the surface of the magnetic nanoparticles. Moreover, the application of an alternating magnetic field in the hybrid system containing magnetic nanoparticle leads to heat generation, which could drive the swelling transition of the polymer.

Comparing the results obtained during about 100 minutes of both assays (with and without the influence of an external

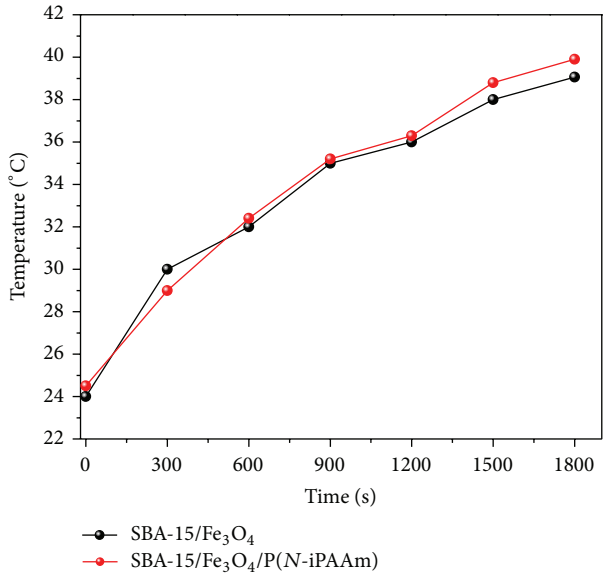

FIGURE 10: Heating induced by magnetic field of SBA-15/Fe_3O_4 and [SBA-15/Fe_3O_4/P(*N*-iPAAm)] systems.

magnetic field), we can observe that the presence of magnetic field affects the release profile of both samples. Even though there is an increase in the drug release rate for the nanocomposites in the presence of the magnetic field ranging from 32 to 40%, this increase is significantly higher for samples containing the polymer. The analysis of the performance of the hybrid system as a drug delivery device in the presence of alternating magnetic field shows that the release profiles vary from approximately 40 to 70%, indicating that the polymer expanded and consequently presented a lesser barrier to the diffusion of atenolol.

These observations lead us to suggest that the drug release response of hybrid systems depends on temperature and the polymer phase behavior. In this case, a synergistic effect of hyperthermia and controlled drug delivery for a hybrid system composed by the combination of SBA-15, Fe_3O_4 nanoparticles, and P(*N*-iPAAm) has occurred. To accomplish this assumption, heating generation experiments were performed and discussed below.

3.3. Magnetic Hyperthermia. The saturation magnetization of SBA-15/Fe_3O_4 is 2 emu/g which is much smaller than that of pure bulk magnetite (94 emu/g) [29] because the nanoscale particles form a single magnetic domain that do not communicate/interact due to coating of silica. The magnetic properties obtained by ^{57}Fe Mössbauer spectroscopy (not shown) showed that the nanocrystals present superparamagnetic characteristics. The AC magnetic field-induced heating characteristics of the nanocomposite and hybrid system in 20 mg·mL^{-1} solution were measured to assess its possible application as a hyperthermia agent in an *in vivo*-like environment. Figure 10 shows the time-dependent temperature curves of the pure and hybrid systems for 222 kHz and 126 Oe AC. When the samples were exposed to an AC magnetic field for 30 min, the temperature ranged from 24 to 39°C and from 24 to 40°C for SBA-15/Fe_3O_4 and [SBA-15/Fe_3O_4/P(*N*-iPAAm)], respectively, showing no statistically significant differences in the temperature variation.

The measured temperatures of the hybrid system suspension after sonication and under 126 Oe AC magnetic fields after 30 min of assay, presented a ΔT_{max} of 16°C. For all evaluated samples, (T + ΔT_{max}) was minor than the recommended hyperthermia treatment temperature, which is reported between 40 and 45°C [30]. At these temperatures, the growth of cancerous cells can be halted and any damage to healthy cells can be avoided by using magnetic nanoparticles with controlled temperatures. It is available treatment when tumors have not metastasized and their locations are known. However, based on such results, it does not mean that the obtained material cannot be used for such application, but the experimental conditions employed to evaluate its heating might be improved.

Thus, a temperature variation of ΔT_{max} = 5–8°C would be sufficient, based on a body temperature of 37°C. Significant results were obtained in our previous work [25]. Hyperthermia tests have demonstrated a good heating capacity of the powders prepared from SiO_2-Fe_3O_4 nanocomposite, which increased linearly with milling time. In the selected experimental conditions, the measured temperatures of the nanoparticle suspension after sonication and under 168 Oe AC magnetic field increased to 47.5°C after 30 min of assay, presenting a ΔT_{max} of 24.5°C. The effect of frequency for $CoFe_2O_4$ nanoparticles dispersed in water on magnetic heating was investigated using a magnetic field of 385 Oe at frequencies of 195, 231, and 266 kHz. The results show that the heating rates diminished with time and reached steady-state temperatures around 30–35°C and ΔT increased linearly with frequency. As a result, heat generation can be controlled in selected magnetic particles by adjusting the magnetic field and frequency [31, 32].

The above results show that the sample prepared in this work is important to be used in a medical application, as drug delivery and magnetic hyperthermia. A critical step in the combined therapy is controlled drug release. Although important, these conclusions need a deeper study of heat generation by adjusting the magnetic field, the frequency, and choosing an appropriated medium with different amounts of materials in order to increase ΔT_{max} and it is planned for future work. Due to their mesoporous properties we also envisioned that such system might be further investigated as a theranostic device. The *in vivo* experiments will be conducted and reported in the due course.

4. Conclusion

The possibility to prepare hybrid system to be used as nanoplatform for drug delivery and heating agent in hyperthermia was presented and discussed. We developed an easy and direct synthesis route to obtain hybrid functional nanosystems based on responsive polymer synthesized inside the iron nanoparticle/mesoporous silica nanocomposites. The above results show that the composition and morphology

of carrier materials and the external agents are important factors in influencing the drug delivery performance. Drug release was more effective and faster in alternating magnetic field for both systems. However, a direct comparison of these results indicates that the performance of the hybrid system is more affected by the presence of the magnetic field, resulting in a greater release of the drug, as the polymer expanded and consequently presented a lesser barrier to the diffusion of atenolol. Hyperthermia tests have demonstrated that the temperature variation achieved under selected conditions increased linearly with milling time. The maximum temperature obtained is around 40°C inferior to that recommended for hyperthermia treatment. Therefore, the magnetic field amplitude, the frequency, or both of them might be reduced in order to optimize the use of the obtained hybrid system. In spite of this, we have shown that mesoporous silica-coated magnetite nanoparticles containing stimuli-responsive polymers with especial structural and magnetic characteristics and unobstructed pores seem to be promising material for use in biomedical application presenting synergistic effects of hyperthermia and controlled drug delivery.

Conflict of Interests

The authors declare that there is no conflict of interests regarding the publication of this paper.

Acknowledgments

The authors wish to thank FAPEMIG (Fundação de Amparo a Pesquisa do Estado de Minas Gerais), CNPQ (Conselho Nacional de Desenvolvimento Científico e Tecnológico), and CAPES (Comissão Aperfeiçoamento de Pessoal de Nível Superior) for their financial support.

References

[1] I. W. Hamley, "Nanostructure fabrication using block copolymers," *Nanotechnology*, vol. 14, no. 10, pp. R39–R54, 2003.

[2] G. J. D. A. A. Soler-Illia, C. Sanchez, B. Lebeau, and J. Patarin, "Chemical strategies to design textured materials: from microporous and mesoporous oxides to nanonetworks and hierarchical structures," *Chemical Reviews*, vol. 102, no. 11, pp. 4093–4138, 2002.

[3] W. Paul and C. P. Sharma, "Nanoceramic matrices: biomedical applications," *American Journal of Biochemistry and Biotechnology*, vol. 2, p. 41, 2006.

[4] A. L. Doadrio, E. M. B. Sousa, J. C. Doadrio, J. Pérez Pariente, I. Izquierdo-Barba, and M. Vallet-Regí, "Mesoporous SBA-15 HPLC evaluation for controlled gentamicin drug delivery," *Journal of Controlled Release*, vol. 97, no. 1, pp. 125–132, 2004.

[5] A. Sousa, K. C. Souza, S. C. Reis et al., "Positron annihilation study of pore size in ordered SBA-15," *Journal of Non-Crystalline Solids*, vol. 354, no. 42-44, pp. 4800–4805, 2008.

[6] M. Vallet-Regí, "Mesoporous silica nanoparticles: their projection in nanomedicine," *ISRN Materials Science*, vol. 2012, Article ID 608548, 20 pages, 2012.

[7] A. De Sousa, D. A. Maria, R. G. De Sousa, and E. M. B. De Sousa, "Synthesis and characterization of mesoporous silica/poly(*N*-isopropylacrylamide) functional hybrid useful for drug delivery," *Journal of Materials Science*, vol. 45, no. 6, pp. 1478–1486, 2010.

[8] G. Vilara, J. Tulla-Puchea, and F. Albericioa, "Polymers and drug delivery systems," *Current Drug Delivery*, vol. 9, pp. 1–28, 2012.

[9] L. M. Geever, M. J. D. Nugent, and C. L. Higginbotham, "The effect of salts and pH buffered solutions on the phase transition temperature and swelling of thermoresponsive," *Journal of Materials Science*, vol. 42, no. 23, pp. 9845–9854, 2007.

[10] W.-F. Lee and Y.-H. Lin, "Swelling behavior and drug release of NIPAAm/PEGMEA copolymeric hydrogels with different crosslinkers," *Journal of Materials Science*, vol. 41, no. 22, pp. 7333–7340, 2006.

[11] R. F. S. Freitas and E. L. Cussler, "Temperature sensitive gels as extraction solvents," *Chemical Engineering Science*, vol. 42, no. 1, pp. 97–103, 1987.

[12] C. S. Biswas, V. K. Patel, N. K. Vishwakarma et al., "Synthesis, characterization, and drug release properties of poly(*N*-isopropylacrylamide) gels prepared in methanol-water cononsolvent medium," *Journal of Applied Polymer Science*, vol. 125, no. 3, pp. 2000–2009, 2012.

[13] S. Kralj, M. Drofenik, and D. Makovec, "Controlled surface functionalization of silica-coated magnetic nanoparticles with terminal amino and carboxyl groups," *Journal of Nanoparticle Research*, vol. 13, no. 7, pp. 2829–2841, 2011.

[14] L. A. Harris, J. D. Goff, A. Y. Carmichael et al., "Magnetite nanoparticle dispersions stabilized with triblock copolymers," *Chemistry of Materials*, vol. 15, no. 6, pp. 1367–1377, 2003.

[15] A. K. Gupta and M. Gupta, "Synthesis and surface engineering of iron oxide nanoparticles for biomedical applications," *Biomaterials*, vol. 26, no. 18, pp. 3995–4021, 2005.

[16] G. Bao, S. Mitragotri, and S. Tong, "Multifunctional nanoparticles for drug delivery and molecular imaging," *Annual Review of Biomedical Engineering*, vol. 15, p. 253, 2013.

[17] K. C. Souza, G. Salazar-Alvarez, J. D. Ardisson, W. A. A. Macedo, and E. M. B. Sousa, "Mesoporous silica-magnetite nanocomposite synthesized by using a neutral surfactant," *Nanotechnology*, vol. 19, no. 18, Article ID 185603, 2008.

[18] M. Choi, F. Kleitz, D. Liu, Y. L. Hee, W.-S. Ahn, and R. Ryoo, "Controlled polymerization in mesoporous silica toward the design of organic-inorganic composite nanoporous materials," *Journal of the American Chemical Society*, vol. 127, no. 6, pp. 1924–1932, 2005.

[19] K. S. W. Sing, "Reporting physisorption data for gas/solid systems with special reference to the determination of surface area and porosity," *Pure and Applied Chemistry*, vol. 57, no. 4, pp. 603–619, 1985.

[20] A. Sayari, P. Liu, M. Kruk, and M. Jaroniec, "Characterization of large-pore MCM-41 molecular sieves obtained via hydrothermal restructuring," *Chemistry of Materials*, vol. 9, no. 11, pp. 2499–2506, 1997.

[21] S. J. Gregg and K. S. W. Sing, *Standard Data for Alpha-s Method Comment*, 2nd edition, 1982.

[22] T. Kokubo, H. Kushitani, S. Sakka, T. Kitsugi, and T. Yamamuro, "Solutions able to reproduce in vivo surface-structure changes in bioactive glass-ceramic A-W3," *Journal of Biomedical Materials Research*, vol. 24, no. 6, pp. 721–734, 1990.

[23] A. Pineau, N. Kanari, and I. Gaballah, "Kinetics of reduction of iron oxides by H2. Part I: low temperature reduction of hematite," *Thermochimica Acta*, vol. 447, no. 1, pp. 89–100, 2006.

[24] D. Zhao, Q. Huo, J. Feng, B. F. Chmelka, and G. D. Stucky, "Nonionic triblock and star diblock copolymer and oligomeric sufactant syntheses of highly ordered, hydrothermally stable, mesoporous silica structures," *Journal of the American Chemical Society*, vol. 120, no. 24, pp. 6024–6036, 1998.

[25] K. C. Souza, N. D. S. Mohallem, and E. M. B. Sousa, "Mesoporous silica-magnetite nanocomposite: facile synthesis route for application in hyperthermia," *Journal of Sol-Gel Science and Technology*, vol. 53, no. 2, pp. 418–427, 2010.

[26] V. Antochshuk, M. Kruk, and M. Jaroniec, "Surface modifications of cage-like and channel-like mesopores and their implications for evaluation of sizes of entrances to cage-like mesopores," *Journal of Physical Chemistry B*, vol. 107, no. 43, pp. 11900–11906, 2003.

[27] A. K. Dash and G. C. Cudworth II, "Therapeutic applications of implantable drug delivery systems," *Journal of Pharmacological and Toxicological Methods*, vol. 40, no. 1, pp. 1–12, 1998.

[28] K. C. Souza, J. D. Ardisson, and E. M. B. Sousa, "Study of mesoporous silica/magnetite systems in drug controlled release," *Journal of Materials Science: Materials in Medicine*, vol. 20, no. 2, pp. 507–512, 2009.

[29] B. D. Cullity and C. D. Graham, *Introdution to Magnetic Materials*, IEEE Press Editorial Board, 2nd edition, 2009.

[30] M. Liangruksa, R. Ganguly, and I. K. Puri, "Parametric investigation of heating due to magnetic fluid hyperthermia in a tumor with blood perfusion," *Journal of Magnetism and Magnetic Materials*, vol. 323, no. 6, pp. 708–716, 2011.

[31] G. Baldi, G. Lorenzi, and C. Ravagli, "Hyperthermic effect of magnetic nanoparticles under electromagnetic field," *Processing and Application of Ceramics*, vol. 3, p. 103, 2009.

[32] E. A. Périgo, S. C. Silva, E. M. B. De Sousa et al., "Properties of nanoparticles prepared from NdFeB-based compound for magnetic hyperthermia application," *Nanotechnology*, vol. 23, no. 17, Article ID 175704, 2012.